


Reductions in NO₂ burden over north equatorial Africa from decline in biomass burning in spite of growing fossil fuel use, 2005 to 2017

Jonathan E. Hickman^{a,1} , Niels Andela^{b,2} , Kostas Tsigaridis^{a,c} , Corinne Galy-Lacaux^d, Money Ossohou^e , and Susanne E. Bauer^a

^aNASA Goddard Institute for Space Studies, New York, NY 10025; ^bBiospheric Sciences Laboratory, NASA Goddard Space Flight Center, Greenbelt, MD 20771; ^cCenter for Climate Systems Research, Columbia University, New York, NY 10025; ^dLaboratoire d'Aérodynamique, Université Toulouse III Paul Sabatier/CNRS, 31400 Toulouse, France; and ^eLaboratoire de Physique de l'Atmosphère et de Mécanique des Fluides, Université Félix Houphouët-Boigny, 22 BP 582 22 Abidjan, Côte d'Ivoire

Edited by Christopher B. Field, Stanford University, Stanford, CA, and approved December 4, 2020 (received for review March 4, 2020)

Socioeconomic development in low- and middle-income countries has been accompanied by increased emissions of air pollutants, such as nitrogen oxides [NO_x: nitrogen dioxide (NO₂) + nitric oxide (NO)], which affect human health. In sub-Saharan Africa, fossil fuel combustion has nearly doubled since 2000. At the same time, landscape biomass burning—another important NO_x source—has declined in north equatorial Africa, attributed to changes in climate and anthropogenic fire management. Here, we use satellite observations of tropospheric NO₂ vertical column densities (VCDs) and burned area to identify NO₂ trends and drivers over Africa. Across the northern ecosystems where biomass burning occurs—home to hundreds of millions of people—mean annual tropospheric NO₂ VCDs decreased by 4.5% from 2005 through 2017 during the dry season of November through February. Reductions in burned area explained the majority of variation in NO₂ VCDs, though changes in fossil fuel emissions also explained some variation. Over Africa's biomass burning regions, raising mean GDP density (USD·km⁻²) above its lowest levels is associated with lower NO₂ VCDs during the dry season, suggesting that economic development mitigates net NO₂ emissions during these highly polluted months. In contrast to the traditional notion that socioeconomic development increases air pollutant concentrations in low- and middle-income nations, our results suggest that countries in Africa's northern biomass-burning region are following a different pathway during the fire season, resulting in potential air quality benefits. However, these benefits may be lost with increasing fossil fuel use and are absent during the rainy season.

air pollution | trace gas emissions | biomass burning | sustainable development

Socioeconomic development and population growth in low- and middle-income countries have been widely associated with increased environmental degradation, including rapid increases in emissions of air pollutants (1–3). In contrast, in countries with a high per capita gross domestic product (GDP), various socioeconomic, institutional, and regulatory factors often cause economic growth to be accompanied by reductions of some pollutant emissions, though these emissions may simply be outsourced to lower income countries (4). The relationship between income level and environmental pressure—known as the Environmental Kuznets Curve—has often been conceptualized as an inverted U-shaped curve, but a wide array of functional relationships is possible (3). For emissions of air pollutants, the relationship has generally been described as an inverted U-shaped curve, though carbon dioxide generally does not follow such a curve (3, 5). Some researchers argue that low- and middle-income countries can mitigate or shorten the period of rapid emissions growth that tends to accompany socioeconomic development for at least some pollutants (4). Africa, and sub-Saharan Africa in particular, is characterized by countries with

low but growing per capita GDP and rapid population growth, which have been linked to increases in emissions of carbon dioxide and particulate matter (6). As these countries continue their trajectories of economic development, emissions of air pollutants from fossil fuel and biofuel combustion are expected to experience explosive growth (7).

Nitrogen dioxide (NO₂) is a reactive gas and air pollutant with a lifetime in the atmosphere on the order of hours (8). In the atmosphere, NO₂ interconverts rapidly with nitric oxide (NO), and the two species are collectively referred to as NO_x. NO₂ itself is toxic, is regulated by the US Environmental Protection Agency, and has been associated with premature mortality and asthma [though its direct effects on health are not clear (9) and it may instead function as a proxy for other pollutants, such as ozone and aerosols that have direct health and mortality impacts (10)]. NO_x is also a key precursor to the formation of tropospheric ozone (O₃), which is damaging to both crop productivity and human health; anthropogenic O₃ contributes to roughly half a million premature deaths annually, of which nearly 20,000 are in Africa (11). In addition, NO_x is involved in reactions with atmospheric ammonia (NH₃) to form nitrate aerosols, which

Significance

Socioeconomic development in low- and middle-income countries is thought to increase emissions of air pollutants, such as nitrogen dioxide (NO₂). In Africa, fossil fuel use has nearly doubled since 2000, but vegetation fires—which cause substantial NO₂ pollution—have declined, partly as a result of human activity. Satellite observations show that during the biomass burning season, NO₂ concentrations in Africa's northern fire region declined by 4.5% between 2005 and 2017, potentially benefitting hundreds of millions of people. Statistical modeling suggests that this decline is associated with declining vegetation fires. During the biomass burning season, higher levels of economic productivity are associated with lower NO₂ concentrations, suggesting that socioeconomic development in this region is resulting in net improvements to air quality.

Author contributions: J.E.H. and N.A. designed research; J.E.H., N.A., K.T., C.G.-L., M.O., and S.E.B. discussed study design; J.E.H. performed research; J.E.H. and N.A. analyzed data; and J.E.H., K.T., C.G.-L., M.O., and S.E.B. wrote the paper.

The authors declare no competing interest.

This article is a PNAS Direct Submission.

Published under the PNAS license.

¹To whom correspondence may be addressed. Email: jonathan.e.hickman@nasa.gov.

²Present address: School of Earth and Ocean Sciences, Cardiff University, Cardiff, CF10 3AT, United Kingdom.

This article contains supporting information online at <https://www.pnas.org/lookup/suppl/doi:10.1073/pnas.2002579118/-DCSupplemental>.

Published February 8, 2021.

contribute to particulate matter pollution (12) as well as in reactions with volatile organic compounds (VOCs), which form organic nitrates (13). Because of the short lifetime of NO_2 , and because it can function as an indicator for other pollutants, it can serve as an indicator of overall changes in air quality.

NO and NO_2 are emitted from a variety of natural and anthropogenic sources. Fossil fuel combustion and anthropogenic alterations to soils through fertilization or livestock management are the primary sources of NO_x in many parts of the world. In sub-Saharan Africa (excluding South Africa), fossil fuel combustion and fertilizer use has been considerably lower than elsewhere, and natural soils and biomass burning have historically been more important sources (14). This is true even in Nigeria (15), which experiences substantial emissions of VOCs from the oil and gas industry (16). NO_x emissions from Lagos have been shown to be either lower than (15) or comparable to other megacities (17), and NO_2 concentrations are generally low during the rainy season, but air quality can become heavily degraded during the biomass burning season (15, 18). However, fossil fuel combustion in the region nearly doubled between 2000 and 2016 (19) and associated emissions of NO_x are projected to

increase sixfold by 2030 in the absence of regulation, as compared to 2005 levels (7).

This increase in fossil fuel combustion is occurring against the backdrop of Africa's unique, fire-prone savanna ecosystems, home to 70% of the global area burned each year (20). Biomass burning in Africa is estimated to be responsible for NO_x emissions of roughly 4 Tg N-yr^{-1} , equivalent to about half of all NO_x emissions for the continent (21), and one third to half of NO_x emissions from biomass burning globally (21–23). The majority of biomass burning in Africa occurs in northern and southern bands of savanna, savanna-forest mosaic, and woodland ecoregions, with a seasonality that follows the migration of the intertropical convergence zone.

The early part of the 21st century has been accompanied by a global decline in burned area, with some of the largest declines occurring in Africa's northern fire band (24). Some of the burned area decline in the northern fire band can be attributed to changes in precipitation that, in turn, affect the quantity and moisture content of available fuels (24–26). However, active anthropogenic suppression of fire has also played an important role (24, 25). Burning is thought to be used as a management strategy—among other uses, humans ignite fires to mineralize

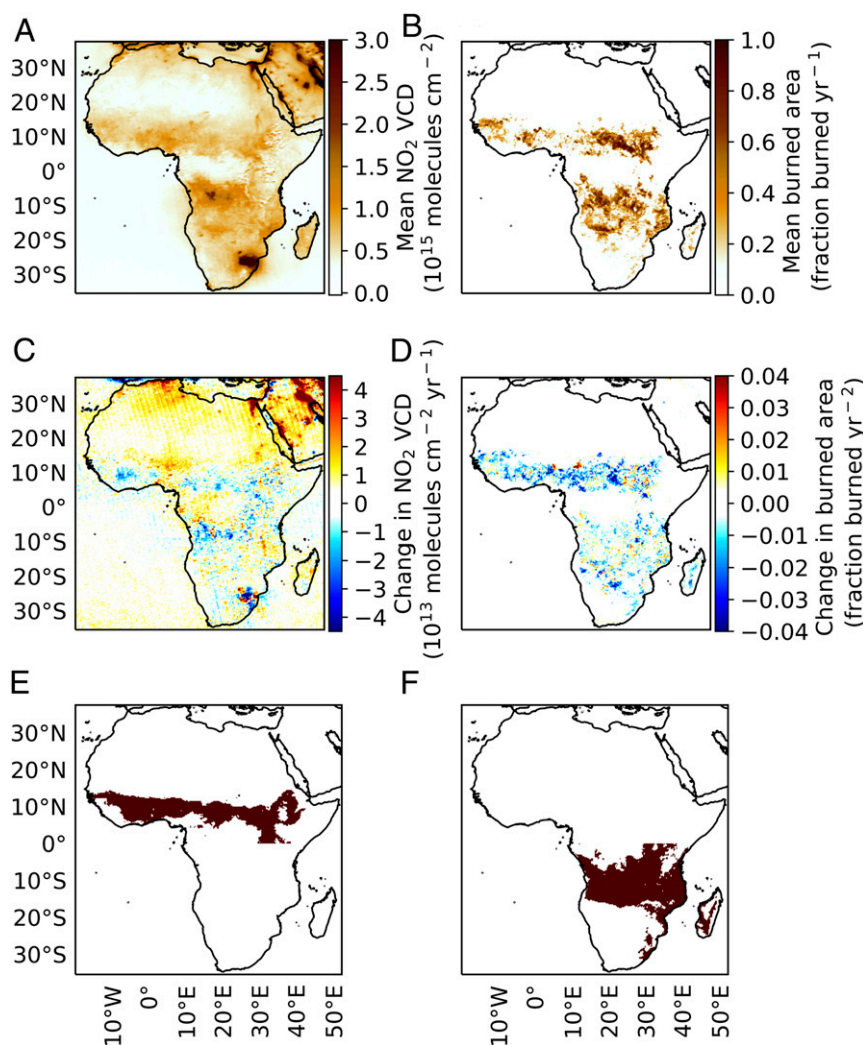


Fig. 1. Long-term annual mean and trends in burned area and tropospheric NO_2 VCDs over Africa for the period 2005 through 2017. (A) Mean annual tropospheric NO_2 VCDs, (B) mean annual burned area, (C) change in mean annual NO_2 VCDs, and (D) change in mean annual burned area. Mask used for analyses of productive savanna in north equatorial Africa (E) and productive savanna in south equatorial Africa (F). The area is defined as including pixels where mean annual precipitation for 2000 to 2017 is $>750 \text{ mm-yr}^{-1}$ and $<1,500 \text{ mm-yr}^{-1}$.

nutrients, improve grazing, and reduce fuel loads and the potential for large, uncontrolled fires (27). Increased population density and the introduction of agricultural land into African savanna landscapes—reflecting socioeconomic transitions from traditional nomadic pastoralist lifestyles (28)—have been associated with a sharp decrease in burned area as people either reduce ignition or suppress fires to protect villages and farms, with a reduction in the amount of pasture area to be maintained (25).

Unfortunately, sub-Saharan Africa remains a severely understudied region—for example, agricultural soil NO fluxes have only been measured directly for two sites (29, 30), and surface air quality monitoring is extremely limited compared to other parts of the world (31). Remote sensing products provide an important tool for filling some of these data gaps. The short NO₂ lifetime in the planetary boundary layer makes it possible to use satellite observations to directly evaluate emissions sources, especially in regions with high temperatures, which tend to shorten the NO₂ lifetime, and in relatively polluted regions, where total column densities and surface emissions are highly correlated (ref. 8 and references therein). Although recent remote sensing work has evaluated long-term trends in NO₂ concentrations around the world, recent trends in the biomass burning region of northern Africa have not been explicitly evaluated, and the relative impacts of socioeconomic development—the possibility of reduced NO_x emissions because of anthropogenic fire suppression and of increasing NO_x emissions from growing fossil fuel use—remain unknown. In general, studies on global trends in NO₂ tend not to focus on Africa, likely because the regions with the highest NO₂ concentrations are in China, Europe, and the United States (e.g., refs. 1, 21). Some earlier studies observed a decline in NO₂ VCDs over north equatorial Africa (32, 33), but others did not (34). These and other large-scale studies (e.g., refs. 8, 34, 35) did not identify mechanisms for the observed NO₂ dynamics, but rather focused on understanding anthropogenic influences on trends in other regions.

Indoor air pollution from biomass combustion for fuel is an important health concern (36). We do not focus on this source. Biofuel combustion is responsible for emissions of 0.6 Tg NO annually across all of Africa (37), which is less than 10% of the magnitude of landscape biomass burning emissions estimated by the Global Fire Emissions Database version 4s [GFED4s (38)] and represents a much smaller proportion of NO_x emissions from landscape biomass burning regions during the dry season.

Here, we use observations of NO₂ by the Ozone Monitoring Instrument [OMI (39)] and burned area from the Moderate Resolution Imaging Spectroradiometer [MODIS (40)] to demonstrate that the recent decline in burned area in the productive savannas of north equatorial Africa—home to over 275 million people—is associated with large declines in tropospheric NO₂ VCDs during the biomass burning season from 2005 through 2017, though positive trends explained in part by increasing fossil fuel combustion were observed in other seasons, especially over Nigeria.

Results and Discussion

High levels of mean annual burned area and tropospheric NO₂ VCDs are clearly observed in the MODIS and OMI data across the northern and southern biomass burning regions of Africa; elevated mean annual tropospheric NO₂ VCDs can also be observed over an array of coal-fired power plants in the South African Highveld (Fig. 1 *A* and *B*).

There is also a clear and broadly spatially consistent negative trend in mean annual tropospheric NO₂ VCDs and burned area across the biomass burning band north of the equator (Fig. 1), which is consistent with other satellite products (*SI Appendix, Figs. S1 and S2*). The decline is especially pronounced during the biomass burning season of November through February (Fig. 2*C*), when mean NO₂ VCDs declined by 0.35%·yr^{−1} or

2.3×10^{11} molecules cm^{−2}·yr^{−1} across that northern band. The burned area trends in this region are broadly similar to those described previously (24, 25). The pattern of declining NO₂ VCDs in north equatorial Africa exhibits a close spatiotemporal correspondence to the decline in burned area (Figs. 2 *C* and *E* and 3). Mean NO₂ VCDs during the rainy season months of May through August—when biomass burning is absent—are less than half the mean for November through February, though NO₂ VCDs increased by roughly 0.63%·yr^{−1}, or 1.65×10^{11} molecules cm^{−2}·yr^{−1}, during this period (Fig. 2 *C* and *D*).

We used multiple linear regression models to investigate the contributions of biomass burning and fossil fuel emissions to observed spatiotemporal variation in tropospheric NO₂ VCDs per 3° × 3° region. During the biomass burning season, changes in NO₂ VCD anomalies across north equatorial Africa are well explained by changes in burned area anomalies (Fig. 3*C*). Changes in NO₂ VCD anomalies in high population density coastal regions are often associated with changes in fossil fuel emission anomalies (Fig. 3*D*). During the May through August period, burned area anomalies explained little of the change in NO₂ VCD anomalies north of the equator, but they explained a large proportion of change in NO₂ VCD anomalies in the southern biomass burning region (Fig. 3*G*). Changes in fossil fuel emission anomalies also explained some of the change in NO₂ VCD anomalies over West Africa during this period. Although the multiple regression model does not explain all of the variation in NO₂ VCD anomalies, it does suggest that biomass burning reductions in north equatorial Africa were the primary driver of declining NO₂ VCDs (*SI Appendix, Fig. S3* and Fig. 3). This conclusion is supported by sensitivity analyses using an Earth system model, in which the NO₂ trend during November through January is highly sensitive to biomass burning NO₂ emissions (*SI Appendix, Figs. S9–S14*). However, increases in NO₂ VCDs—particularly during the rainy season—can be observed in West Africa and in Nigeria, where economic growth has been substantial (<https://data.worldbank.org>).

Examining the relationship between GDP and NO_x emissions or tropospheric NO₂ VCDs helps illustrate the net influence of economic development and human activity on atmospheric composition. Spatial patterns in long-term annual mean emissions from inventories show clear relationships with GDP density (GDP·km^{−2}) in the northern biomass burning region (Fig. 4 *A–C*): As GDP density increases, NO_x emissions from fossil fuel combustion tend to increase during both seasons, and emissions from biomass burning tend to decrease during the biomass burning season. When looking at biomass burning and fossil fuel emissions combined, NO_x emissions decrease in response to increasing GDP density when it is below \$300,000 USD·km^{−2} and increase above that threshold; the same pattern broadly holds for tropospheric NO₂ VCDs. However, the emissions inventories appear to substantially underestimate the mitigating effect of increasing GDP density on NO_x emissions during the biomass burning season. According to the inventories, at GDP densities of roughly \$500,000 USD·km^{−2} or above—which covers 45% of the region's population—NO_x emissions are larger than those at the lowest level of GDP density. At the highest level of GDP density, inventory NO_x emissions are three times higher than at the lowest GDP density level. In contrast, OMI suggests any increase in GDP results in lower NO₂ VCDs than at the lowest level of GDP density (Fig. 4*B*). However, it should be noted that the overall relationship is U-shaped, and, at the two highest GDP density levels, NO₂ VCDs approach background levels. These two highest levels of GDP density represent a total of 15.6% of people in the northern productive savannas—a substantial minority. Although the NO₂ VCDs are influenced by additional emission sources and atmospheric processes, the pattern derived from OMI observations suggests that changes in biomass burning play a more important role in determining atmospheric composition

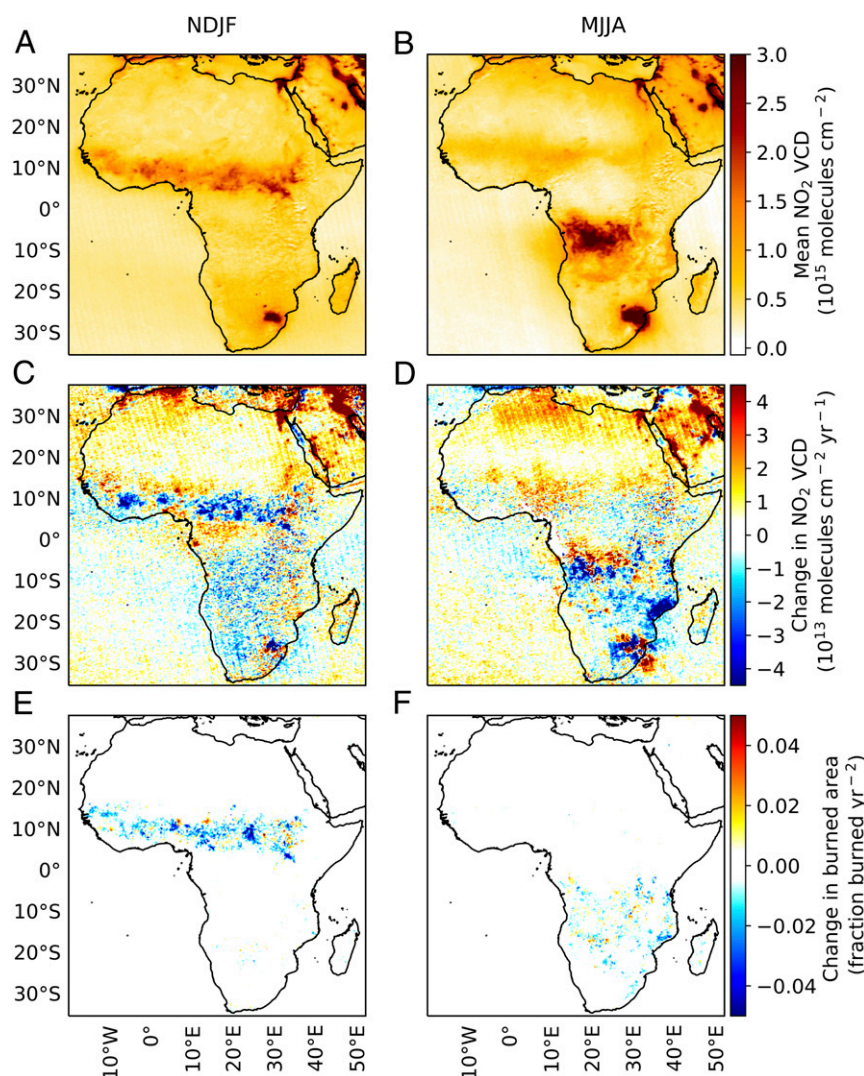


Fig. 2. Long-term annual mean NO_2 VCDs and trends in burned area and tropospheric NO_2 VCDs over Africa during the northern and southern biomass burning seasons for the period 2005 through 2017. Mean tropospheric NO_2 VCDs during November through February (NDJF) (A) and May through August (MJJA) (B). Change in mean tropospheric NO_2 VCDs during NDJF (C) and MJJA (D). Change in mean burned area during NDJF (E) and MJJA (F).

than expected by the inventories alone, consistent with a large unobserved contribution of fire emissions from small fires (41). When comparing these relationships at the beginning and end of the time series, we find that the overall U-shape does not change qualitatively (*SI Appendix, Figs. S4 and S5*).

We do not observe a decline in NO_2 or an overall negative relationship between NO_2 VCDs and GDP density during either the dry or rainy season in the southern biomass burning region (*SI Appendix, Fig. S6*). The southern biomass burning region has not experienced the expansion of agriculture and associated reduction in burned area and has experienced increases in burned area linked to changes in the Multivariate El Niño-Southern Oscillation (ENSO) Index (24, 25). We also expect that the specific relationship between GDP density and NO_2 VCDs observed in the northern biomass burning region may be unique to regions with large biomass burning emissions.

During the rainy season when biomass burning is absent, both emissions inventories and OMI observations reveal a pattern consistent with traditional expectations: emissions and VCDs increase with increasing GDP density (Fig. 4 G–J). However, the NO_2 VCDs during the rainy season tend to be substantially lower than during the dry season. The same general relationships for

both seasons can also be observed for the southern biomass burning region (*SI Appendix, Fig. S6*).

Particularly, given previous evidence that socioeconomic development has been an important driver of recent declines in biomass burning across the region (24; Fig. 1C), we believe these spatial and temporal relationships strongly suggest that socioeconomic development has been driving a decline in NO_2 VCDs over north equatorial Africa during the biomass burning season (2). The reduction in NO_2 VCDs appears to be a consequence of the fact that economic development is occurring in an atmospheric environment that is already heavily polluted during the dry season, as a result of the fire cycle. For example, during the dry season, urban environments in Nigeria have uniformly unhealthy NO_2 concentrations (42–45), but the air is relatively clean during the rainy season, outside of major traffic intersections (46, 47). In this context, the net effect of socioeconomic development is to reduce NO_2 concentrations during the most polluted months of the year, when health impacts can be expected to be greatest, though note that these reductions may be largely absent in locations with the highest levels of GDP density, reflecting the U-shaped curve (Fig. 4B). Ultimately, it is possible that in this biomass burning region, the Environmental

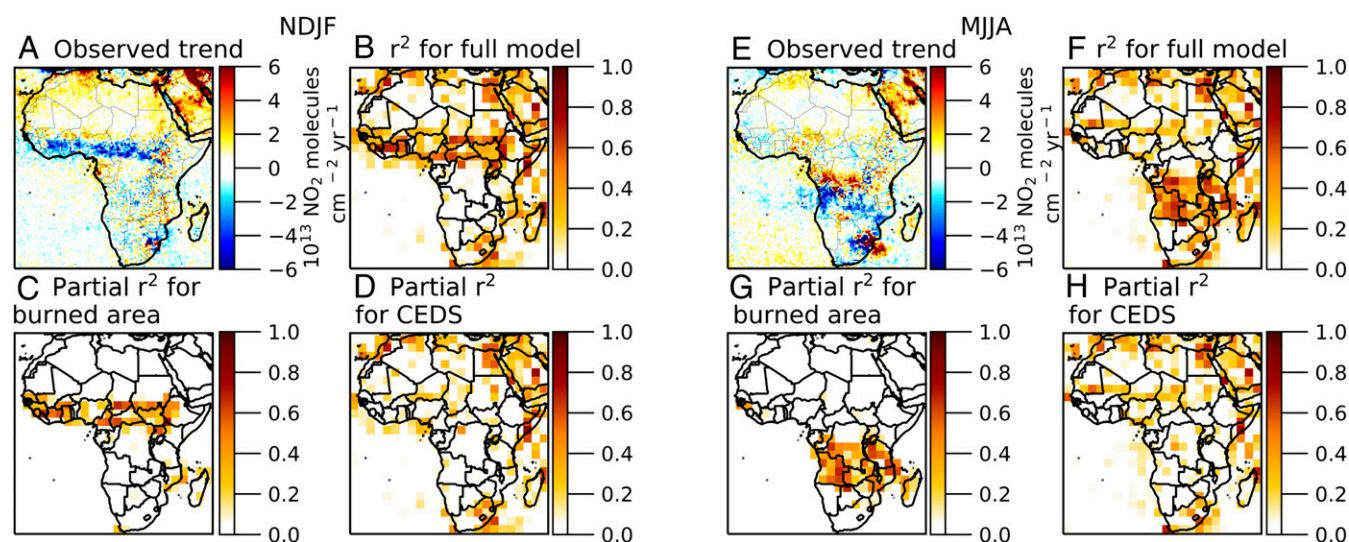


Fig. 3. Much of the variation in NO₂ VCDs over biomass burning regions during the fire season is explained by variation in burned area. Trend in tropospheric NO₂ VCDs during November through January (NDJF) (A). R^2 for multiple regression relating spatiotemporal variation in burned area and fossil fuel emissions to NO₂ VCDs in $3^\circ \times 3^\circ$ grid cells for NDJF (B). Coefficient of partial determination for the effects of burned area during NDJF (C) and for the effects of fossil fuel emissions during NDJF (D). The results of the same analyses for May through August (MJJA) are presented in E–H: NO₂ trends (E), R^2 for the relationship between burned area and fossil fuel emissions (F), and coefficients of partial determination for the effects of burned area (G) and of fossil fuel emissions (H). Fossil fuel emissions are from CEDS.

Kuznets Curve will emerge as an inverted N-shaped relationship (3), with the initial decline in NO₂ emissions from reduced biomass burning associated with growing GDP ultimately being offset by increases in fossil fuel emissions accompanying additional GDP growth and then mitigation of those emissions with further GDP increases.

It is worth noting that there are exceptions to the overall relationship between burned area and NO₂ VCDs in north equatorial Africa. Patches of positive NO₂ VCDs and burned area trends occur during the dry season throughout the northern fire band, particularly in the Central African Republic and South Sudan (Fig. 2 C and E). These countries have widespread agropastoralism and little cropped area (48) and may experience less agriculturally related fire suppression. There are also two hotspots of burned area increases in northern Nigeria during the dry season. The western hotspot is spatially coincident with an area of cropland expansion and may reflect land clearing practices (49).

Interestingly, although the mean seasonal trend for November through February is negative, monthly trends for NO₂ and NH₃ VCDs are positive in February (Fig. 5 and *SI Appendix, Fig. S7*). These positive trends likely result from small fires associated with agricultural field preparation in anticipation of planting in March and April (49, 50), with both expansion of agricultural area as well as increased fuel generated from higher crop productivity responsible for the positive trend (48). There is an observed decline in burned area during February from MODIS, but it is small and spatially inconsistent (*SI Appendix, Fig. S8*) and MODIS is known to miss burned area from small fires such as those typical of agricultural burning: It underestimated burned area across Africa's northern biomass burning region during February and March 2016 by a factor of 3 to 6 (41).

Other factors could potentially contribute to the NO₂ VCD trend observed during the northern hemisphere dry season. Lightning represents a relatively minor source of NO_x in Africa, particularly during the dry season (14, 21). Reliable observational constraints on lightning trends do not exist for Africa (51), but thunderstorm frequency has been found to be increasing (52, 53) and so lightning is unlikely to explain negative NO₂ VCD

trends. Consistent changes in transport could also result in concentration trends. We evaluated a 10-member ensemble of simulations using the GISS ModelE2.1, which provides a range of plausible wind speeds and directions and find that the NO₂ trend is insensitive to this variation (*SI Appendix, Fig. S12*). Convective activity is low during November through February in north equatorial Africa and trends in annual convection in the region are small, especially in comparison with other parts of Africa (54). Systematic changes in Air Mass Factors (AMFs) over time could conceivably result in apparent VCD trends, but the OMI Standard Product (SP) version 3 AMFs do not exhibit clear, spatially consistent trends (*SI Appendix, Fig. S15*). It is also conceivable that a reduction in combustion efficiency could contribute to the negative trend in NO₂ VCDs. A reduction in combustion efficiency would be expected to be accompanied by increases in emissions of less oxidized forms of N, such as NH₃, but NH₃ VCDs also decreased when NO₂ VCDs decreased in the northern biomass burning region (Fig. 5), consistent with an overall decline in biomass burning. Although there were increasing trends of CO VCDs during all months (Fig. 5), they likely result from emissions from woodier biomes: CO has a much longer atmospheric lifetime than NH₃ or NO₂ and transport plays a more important role in determining local CO concentrations. Lastly, it is possible that changes in NO_x chemistry could influence its lifetime and affect concentration trends. Earth system model analyses suggest that the trend in NO₂ VCDs is a direct consequence of changes in biomass burning emissions and changes in chemistry are unlikely to contribute to the trend in any meaningful way (*SI Appendix, Figs. S9–S14*).

Soils are an important source of NO_x in north equatorial Africa (21) and can be expected to contribute to variability in NO₂ VCDs during the rainy season. Fertilizer use is not currently expected to contribute to substantial NO_x emissions (29). Although fertilizer use is reported to be increasing in many countries in percentage terms, the absolute changes are small (<https://data.worldbank.org>) and the reliability of reported data are under question (55). Our observations of increasing NO₂ VCDs during April and May (*SI Appendix, Fig. S7*) suggest that there may be an increase in soil emissions associated with agriculture

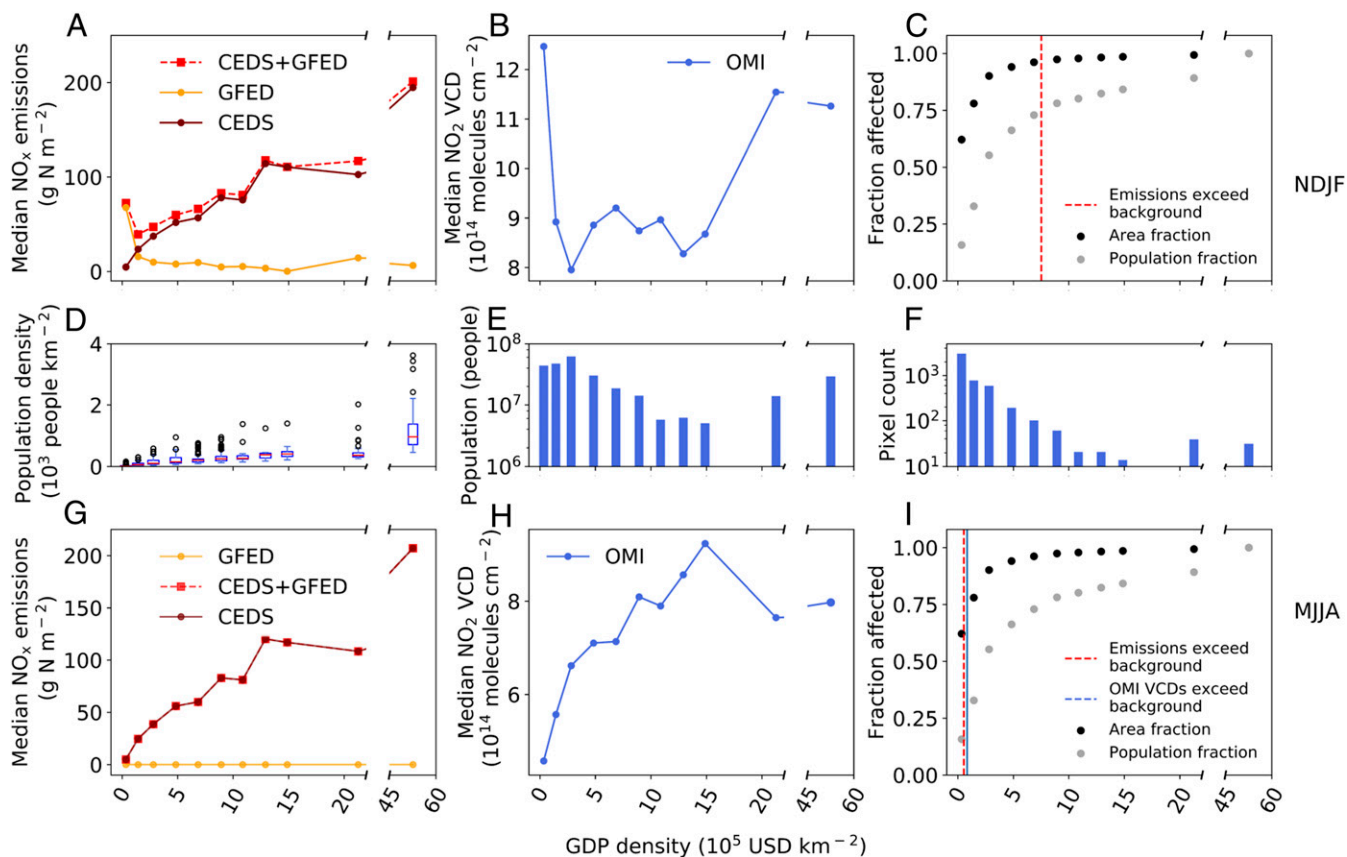


Fig. 4. The relationship between GDP density and inventory NO_x emissions or satellite observations of tropospheric NO_2 VCDs in the north equatorial productive savannas of Africa (Fig. 1E) for the dry season (A–C), information on the affected population and area (D–F), and relationship between GDP density and inventory NO_x emissions or satellite observations of tropospheric NO_2 VCDs during the rainy season (G–I). (A and G) Variation of median inventory estimates of biomass burning and fossil fuel NO_x -N emissions with GDP density. (B and H) Variation of median tropospheric NO_2 VCDs with GDP density. (C and I) Cumulative land area and population fraction represented with increasing levels of GDP density. Vertical lines represent the GDP density at which NO_2 emissions exceed levels in the lowest GDP density bin; note that there is no such point for NO_2 VCDs in C. Median, quartiles, and outliers for population density (D), total population (E), and the number of pixels per GDP density bin are based on spatial data from 2013.

or changes in emissions of NO from natural soils at the onset of the rainy season (21, 56, 57).

Although there is a clear relationship between the burned area and tropospheric NO_2 VCD anomalies during May through August in the southern biomass burning region (Fig. 3G), both the burned area trends and the tropospheric NO_2 VCD trends in the region tend to be more variable than in the northern region (Fig. 2D and F). The overall trend in the southern region may also be influenced in part by the 2015 to 2016 El Niño: In the more arid grasslands of Botswana, Namibia, and Angola, where the negative trends are most prominent, interannual variability in burned area is strongly influenced by the ENSO cycle. During El Niño years, such as 2015 and 2016, dry conditions during the growing season result in lower fuel loads and less biomass burning during the subsequent dry season (24, 25, 33, 58).

Conclusion

The expansion of population and agriculture across north equatorial Africa has been a major driver of a decline in biomass burning activity during the early 21st century through changes in human land management in the region (24, 25). At the same time, fossil fuel use has expanded rapidly in the region. Here, we show that, across the northern fire band, the net effect of these contrasting regional forces is a decline in mean tropospheric NO_2 VCDs on the order of $0.35\% \cdot \text{yr}^{-1}$ during the biomass burning season, roughly proportional to the $0.6\% \cdot \text{yr}^{-1}$ decline in burned area in the region between 2005 and 2017. These results

suggest that increases in NO_x emissions from fossil fuel use are more than offset by the decline in emissions from biomass burning during the dry season. This sets many African nations on a unique pathway where ongoing socioeconomic development may result in improved regional air quality during the most polluted months of the year. However, it is important to note that population growth in sub-Saharan Africa is rapid and has outpaced growth in fossil fuel use (59), creating a large potential for emissions growth as economic growth enables greater per capita fuel use, particularly in densely populated urban areas (7). Indeed, we find that continued economic development appears likely to be accompanied by increases in NO_2 pollution during rainy season months, and grid cells with the highest levels of GDP density have relatively high NO_2 VCDs during the biomass burning season. With continued increases in fossil fuel emissions, anthropogenic NO_2 emissions may become the dominant source of NO_x throughout the year and, barring efforts to mitigate emissions, further development would be accompanied by NO_x concentrations higher than are currently found on the continent. It is also important to note that although the decrease in biomass burning may be beneficial to human health, it can be disastrous for ecosystems and species that depend on fire as part of their natural ecology (60).

Materials and Methods

Observations and Data. We used NASA's level 2 tropospheric NO_2 column density SP version 3 from OMI aboard NASA's Aura satellite, launched in July

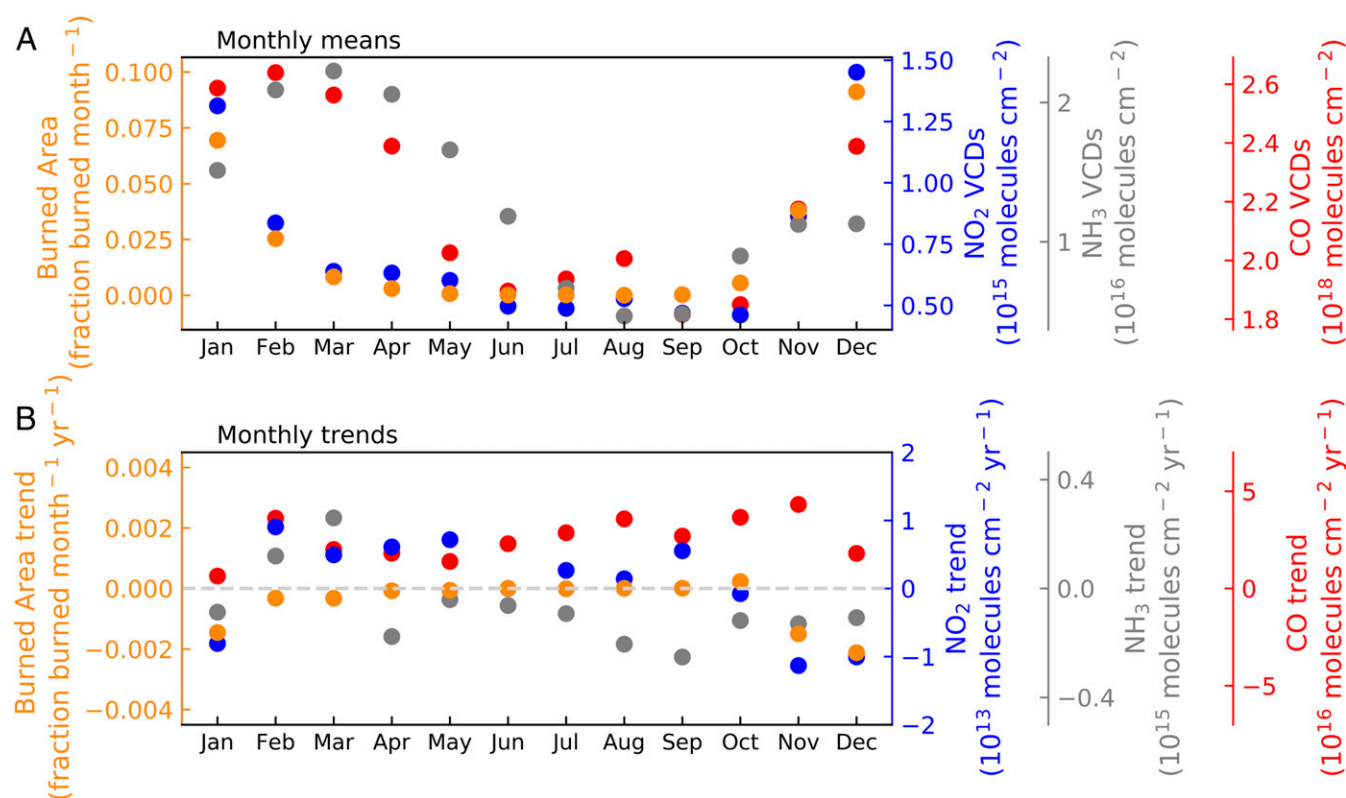


Fig. 5. Monthly means (A) and trends (B) of NO₂ VCDs, NH₃ VCDs, CO VCDs, and burned area for fire-prone ecoregions in north equatorial Africa for 2008 through 2017. The dashed gray line in B represents zero change. Values are for pixels where mean annual precipitation ranges from 750 to 1,500 mm·yr⁻¹, shown in Fig. 1E.

2004. OMI is a nadir-viewing spectrometer, which measures solar backscatter in the ultraviolet-visible range (61). Starting in 2007, the quality of level 1B radiance data for some OMI viewing directions has been affected, also known as the row anomaly. The affected rows vary over time; we have limited our analysis to observations from rows 5 through 23, which have been unaffected by the row anomaly over the entire lifetime of the instrument (39). We also included only observations that were at least 70% cloud-free, had a solar zenith angle under 80, had terrain reflectivity of less than 0.3, and were otherwise free from error flags. Negative NO₂ column values were included in the calculation of means and errors to avoid the introduction of bias. The screened observations were regridded to 0.25° resolution. Specifically, we overlaid a subscale grid with a resolution of 0.02° × 0.03° centered over each observation and extending over the entire elliptical satellite footprint. We added the observation value of the footprint for subscale grid cells within the observation to its corresponding 0.25° grid cell, weighted by the number of subscale observations included in the larger grid cell. Only subscale grid cells that are entirely within an OMI observation were assigned an observation value, and only subscale grid cells that are entirely within a 0.25° grid cell are used to calculate its value.

The OMI NO₂ product relies on air mass factors, which are calculated using an atmospheric chemical transport model; as a consequence, the OMI product is sensitive to model representations of the atmosphere. These data are not well constrained in regions such as sub-Saharan Africa, which are not frequently analyzed in chemical transport models (8, 62).

OMI's level 2 NO₂ product has been validated against in situ and surface-based observations (63), and the level 3 product has shown good agreement with surface observations at six sites in West and Central Africa (64). Random uncertainty in the OMI NO₂ SP version 3.1 data has been given as 1.0×10^{15} molecules·cm⁻², equivalent to roughly 10 to 20% in polluted areas (39). Random errors are assumed to cancel out in our trend analysis, since the response variable is an annual (or seasonal) average of observations. Assuming random errors cancel out, only systematic errors related to AMFs and tropospheric vertical column contents remain. These errors have been assigned an uncertainty of 20% (62), though AMFs are not as well constrained in sub-Saharan Africa, which is not frequently analyzed in chemical

transport models (8, 62). The reliance on nearly cloud-free grid cells may introduce bias, since greater sunlight in these grid cells may induce higher photochemical rates. However, north equatorial Africa in particular, and Africa in general, have experienced small or nondetectable trends in cloud cover—typically less than $\pm 1\%$ ·decade⁻¹ (65). Systematic errors do not contribute to uncertainty in trend analyses. In addition, we first take monthly averages, based on all daily observations within a given month, before calculating seasonal means to minimize any potential effects of temporal variability in cloud cover.

The OMI NO₂ products use an implicit aerosol correction to account for the optical effects of aerosols, but retrievals can be biased when aerosol loading is extreme (e.g., ref. 66). Under these conditions, the OMI NO₂ retrieval is biased low by roughly 20 to 40% (67). Since systematic errors do not contribute to uncertainty in trend analysis, the only source of aerosol-related error in trend analysis would be related to the decrease in biomass burning, estimated at roughly 1%·yr⁻¹ during the OMI lifetime (24) and roughly 0.6%·yr⁻¹ in our analysis of the northern biomass burning region. Note that any aerosol-related error would have the potential effect of biasing trends in a positive direction in regions where biomass burning is decreasing, hence any decreasing NO₂ trends in those regions may be larger than quantified here.

We used measurements of CO and NH₃ from the Infrared Atmospheric Sounding Interferometer (IASI), aboard the European Space Agency's Metop-A launched in 2006. IASI-A is a sun-synchronous polar-orbiting instrument with a spatial resolution of 12 km and swath width of about 2,200 km, resulting in near daily global coverage both during ascending and descending node. Here, we use morning observations (9:30 AM local solar time equator crossing, descending node), when the thermal contrast is more favorable for retrievals (68, 69). For NH₃ we used the Artificial Neural Network for IASI (ANNI-NN) version 2.2R-I retrieval product (70); only retrievals with cloud cover under 10% were used. For CO we used the product obtained with the Fast Optimal Retrievals on Layers for IASI (FORLI) version 20140922 retrieval algorithm (71), using retrievals with cloud cover under 25%.

To evaluate burned area trends, we used the 500 m MCD64A1 collection 6 MODIS burned area product (40). For our analyses, we calculated annual MODIS burned area data from January 2005 through December 2017 at 0.25° resolution. The proportion of the annual burned area for a grid cell was greater than one in three grid cells; in those grid cells the annual burned area value was set to 1.

We also used the Tropical Rainfall Measuring Mission (TRMM) daily precipitation product (3B42), which is based on a combination of TRMM observations, geo-synchronous infrared observations, and rain gauge observations (72). Mean annual precipitation was calculated as the sum of daily precipitation for each year. One year of independent rain gauge observations from West Africa have been used to validate the product at 1° × 1° resolution, with no indication of bias in the product (73).

We used emissions estimates of NO_x from two emissions inventories. GFED4s was used for biomass burning emissions of NO_x [reported as NO (38)]. GFED4s estimates monthly dry matter emissions at 0.25° resolution based on burned area, boosted with estimates of small fire burned area. NO_x emissions are estimated from the dry matter emissions using an emission factor based primarily on ref. 74; we used data for 2005 through 2017. The Community Emissions Data System (CEDS) for Historical Emissions was used for fossil fuel emissions of NO_x [reported as NO₂ (75)]. CEDS provides monthly fossil fuel emissions from eight sectors at 0.5° resolution; we summed emissions from all sectors prior to analysis. We used data for 2005 through 2014, the last year currently available. Emissions from both inventories were converted to units of g NO_x-N m⁻²-s⁻¹.

GDP Density Analyses. We evaluated the spatial relationship between mean annual tropospheric NO₂ VCDs, emissions, and GDP density—or GDP·km⁻²—estimated across the productive savanna regions in Africa. This region was defined as pixels with mean annual precipitation greater than 750 mm·yr⁻¹ and less than 1,500 mm·yr⁻¹, which includes 74% of annual burned area in Africa (Fig. 1). We calculated 0.25° mean population density (people per square kilometer of land) based on the 2013 version of the US Department of Energy's Gridded Landscan population dataset (76). We calculated mean per capita GDP for 2005 to 2014 at a resolution using the gridded GDP_per_capita_PPP_1990_2015 dataset (77) and multiplied it by the population density dataset to obtain GDP density. For each pixel in the masked area, excluding open water grid cells, we calculated mean tropospheric NO₂ VCDs, total NO_x-N emissions from GFED4s, and total NO_x-N emissions from CEDS over 2005 to 2014 (the period for which CEDS data are available) for either November through February or May through August. CEDS data, which are available at 0.5° resolution, were downsampled to 0.25° resolution before masking by setting each 0.25° × 0.25° grid cell to the value of the 0.5° grid cell within which it is contained. We then evaluated the spatial distribution of median NO₂ VCDs and emissions for nine bins of GDP densities; the nine bins encompassed all pixels in our productive savanna regions.

Statistical Analyses. For trend analysis of observations, we used least square linear regression at the 0.25° and 0.5° resolution scale. All analyses were conducted in Python 3.

We also used multiple linear regression models to evaluate how well variation in fossil fuel emissions and burned area explained spatial and

temporal variation in NO₂ VCDs. NO₂ VCDs and burned area were scaled to 0.5° resolution before analysis to match the native CEDS resolution. In order to balance between a well constrained model fit and provide a regional understanding of emissions drivers, we fit multiple linear regression models using data from the 2005 to 2014 period (the only period for which CEDS emissions are available) and across all 0.5° grid cells within each larger 3° × 3° region, excluding open water pixels. In order to increase the model sensitivity to the temporal variability and trends, we modeled the NO₂ relationship with burned area and fossil fuel emissions as a zero-intercept regression of anomalies of NO₂ VCDs as the response variable and anomalies of burned area and anomalies of CEDS fossil fuel emissions as the predictor variables. We modeled these relationships separately for the periods of November through February and May through August and calculated coefficients of partial determination for each predictor variable. For each of these 4-mo periods, we also calculated predicted NO₂ VCD anomalies as the product of the full burned area anomalies (including trend and variation) and the per-grid cell slope between burned area and NO₂ VCD anomalies plus the product of the full fossil fuel emission anomalies (including trend and variation) and the per-grid cell slope between fossil fuel emissions and NO₂ VCD anomalies. We calculated additional predicted NO₂ VCD anomalies using only either the burned area or fossil fuel emission anomalies separately. Observed and modeled trends were estimated based on least square linear regression.

It is important to note that none of our analyses account for potential transport of gases in the atmosphere after emission, which could affect the presence and strength of any spatiotemporal relationships. However, the lifetime of NO₂ in the atmosphere is on the order of hours (78–80) and, as noted above, often exhibits a close spatial coupling with emission sources (8).

Data Availability. All data used are available from public sources. OMI L2 NO₂ SP version 3 is available at https://disc.gsfc.nasa.gov/datasets/OMNO2_003/summary. The TRMM L3 daily precipitation product 3B42 is available at https://disc.gsfc.nasa.gov/datasets/TRMM_3B42_Daily_7/summary. Modern-Era Retrospective analysis for Research and Applications wind data are available at https://disc.gsfc.nasa.gov/datasets/M2TMNXSLV_5.12.4/summary. The IASI ANNI-NNv2.2R-L2 NH₃ product is available at <https://iasi.aeris-data.fr/NH3/>. The IASI FORLI v20140922 CO product is available at https://iasi.aeris-data.fr/CO_IASI_A_data/. The MODIS MCD64A1 collection 6 daily burned area product is available at <https://lpdaac.usgs.gov/products/mcd64a1v006/>. The CEDS anthropogenic NO_x emissions data are available at <https://handle-egsf.dkrz.de/lp21.14100/4f81932b-ee07-42fc-9a7b-3a4aa5c058af>. GFED4s emissions data are available at <https://www.geo.vu.nl/~gwerf/GFED/GFED4/>. The GDP_per_capita_PPP_1990_2015 dataset is available at <https://datadryad.org/stash/dataset/doi:10.5061/dryad.dk1j0>. The US Department of Energy's Gridded Landscan population dataset for 2013 is available at <https://landsat.ornl.gov/downloads/2013>. All other study data are included in the article and/or SI Appendix.

ACKNOWLEDGMENTS. We thank Xiaomeng Jin for sharing data during revision.

1. X. Zhang *et al.*, Long-term trends in NO₂ columns related to economic developments and air quality policies from 1997 to 2016 in China. *Sci. Total Environ.* **639**, 146–155 (2018).
2. T. M. Selden, D. Song, Environmental quality and development: Is there a Kuznets curve for air pollution emissions? *J. Environ. Econ. Manage.* **27**, 147–162 (1994).
3. S. A. Sarkodie, V. Strezov, A review on environmental Kuznets curve hypothesis using bibliometric and meta-analysis. *Sci. Total Environ.* **649**, 128–145 (2019).
4. D. I. Stern, The rise and fall of the environmental Kuznets curve. *World Dev.* **32**, 1419–1439 (2004).
5. Z. Zoundi, CO₂ emissions, renewable energy and the environmental Kuznets curve, a panel cointegration approach. *Renew. Sustain. Energy Rev.* **72**, 1067–1075 (2017).
6. E. S. Osabuohien, U. R. Efofi, C. M. W. Gitau, Beyond the environmental Kuznets curve in Africa: Evidence from panel cointegration. *J. Environ. Policy Plann.* **16**, 517–538 (2014).
7. C. Lioussie, E. Assamoi, P. Criqui, C. Granier, R. Rosset, Explosive growth in African combustion emissions from 2005 to 2030. *Environ. Res. Lett.* **9**, 035003 (2014).
8. N. A. Krotkov *et al.*, Aura OMI observations of regional SO₂ and NO₂ pollution changes from 2005 to 2015. *Atmos. Chem. Phys.* **16**, 4605–4629 (2016).
9. T. W. Hesterberg *et al.*, Critical review of the human data on short-term nitrogen dioxide (NO₂) exposures: Evidence for NO₂ no-effect levels. *Crit. Rev. Toxicol.* **39**, 743–781 (2009).
10. I. Levy, C. Mihelc, G. Lu, J. Narayan, J. R. Brook, Evaluating multipollutant exposure and urban air quality: Pollutant interrelationships, neighborhood variability, and nitrogen dioxide as a proxy pollutant. *Environ. Health Perspect.* **122**, 65–72 (2014).
11. R. A. Silva *et al.*, Global premature mortality due to anthropogenic outdoor air pollution and the contribution of past climate change. *Environ. Res. Lett.* **8**, 034005 (2013).
12. S. E. Bauer, K. Tsigaridis, R. Miller, Significant atmospheric aerosol pollution caused by world food cultivation. *Geophys. Res. Lett.* **43**, 5394–5400 (2016).
13. J. A. Fisher *et al.*, Organic nitrate chemistry and its implications for nitrogen budgets in an isoprene- and monoterpene-rich atmosphere: Constraints from aircraft (SEAC⁴RS) and ground-based (SOAS) observations in the southeast US. *Atmos. Chem. Phys.* **16**, 5969–5991 (2016).
14. L. Jaeglé, L. Steinberger, R. V. Martin, K. Chance, Global partitioning of NO_x sources using satellite observations: Relative roles of fossil fuel combustion, biomass burning and soil emissions. *Faraday Discuss.* **130**, 407–423, discussion 491–517, 519–524 (2005).
15. E. A. Marais *et al.*, Anthropogenic emissions in Nigeria and implications for atmospheric ozone pollution: A view from space. *Atmos. Environ.* **99**, 32–40 (2014).
16. L. C. Osuji, G. O. Awiri, Flared gases and other pollutants associated with air quality in industrial areas of Nigeria: An overview. *Chem. Biodivers.* **2**, 1277–1289 (2005).
17. J. R. Hopkins *et al.*, Direct estimates of emissions from the megacity of Lagos. *Atmos. Chem. Phys.* **9**, 8471–8477 (2009).
18. S. E. Bauer, U. Im, K. Mezuman, C. Y. Gao, Desert dust, industrialization, and agricultural fires: Health impacts of outdoor Air pollution in Africa. *J. Geophys. Res. Atmos.* **124**, 4104–4120 (2019).
19. BP, *BP Statistical Review of World Energy* (BP, London, UK, 2018).
20. I. Alonso-Canas, E. Chuvieco, Global burned area mapping from ENVISAT-MERIS and MODIS active fire data. *Remote Sens. Environ.* **163**, 140–152 (2015).

21. L. Jaeglé *et al.*, Satellite mapping of rain-induced nitric oxide emissions from soils. *J. Geophys. Res. Atmos.* **109**, D16309 (2004).
22. D. R. Cahoon, B. J. Stocks, J. S. Levine, W. R. Cofer, K. P. O'Neill, Seasonal distribution of African savanna fires. *Nature* **359**, 812–815 (1992).
23. S. Whitburn *et al.*, Ammonia emissions in tropical biomass burning regions: Comparison between satellite-derived emissions and bottom-up fire inventories. *Atmos. Environ.* **121**, 42–54 (2015).
24. N. Andela *et al.*, A human-driven decline in global burned area. *Science* **356**, 1356–1362 (2017).
25. N. Andela, G. R. van der Werf, Recent trends in African fires driven by cropland expansion and El Niño to la Niña transition. *Nat. Clim. Chang.* **4**, 791–795 (2014).
26. M. Zubkova, L. Boschetti, J. T. Abatzoglou, L. Giglio, Changes in fire Activity in Africa from 2002 to 2016 and their potential drivers. *Geophys. Res. Lett.* **46**, 7643–7653 (2019).
27. L. J. Shaffer, Indigenous fire use to manage savanna landscapes in southern Mozambique. *Fire Ecol.* **6**, 43–59 (2010).
28. M. D. Turner, The new pastoral development paradigm: Engaging the realities of property institutions and livestock mobility in dryland Africa. *Soc. Nat. Resour.* **24**, 469–484 (2011).
29. J. E. Hickman *et al.*, Nonlinear response of nitric oxide fluxes to fertilizer inputs and the impacts of agricultural intensification on tropospheric ozone pollution in Kenya. *Glob. Change Biol.* **23**, 3193–3204 (2017).
30. F. X. Meixner *et al.*, Preliminary results on nitric oxide emission from a southern African savanna ecosystem. *Nutr. Cycl. Agroecosyst.* **48**, 123–138 (1997).
31. E. Coker, S. Kizito, A narrative review on the human health effects of ambient air pollution in sub-Saharan Africa: An urgent need for health effects studies. *Int. J. Environ. Res. Public Health* **15**, 427 (2018).
32. P. Schneider, R. J. van der A, A global single-sensor analysis of 2002–2011 tropospheric nitrogen dioxide trends observed from space. *J. Geophys. Res. Atmos.* **117**, D16309 (2012).
33. R. J. van der A *et al.*, Trends, seasonal variability and dominant NO_x source derived from a ten year record of NO₂ measured from space. *J. Geophys. Res. Atmos.* **113**, D04302 (2008).
34. A. Richter, J. P. Burrows, H. Nüss, C. Granier, U. Niemeier, Increase in tropospheric nitrogen dioxide over China observed from space. *Nature* **437**, 129–132 (2005).
35. J. A. Geddes, R. V. Martin, B. L. Boys, A. van Donkelaar, Long-term trends worldwide in ambient NO₂ concentrations inferred from satellite observations. *Environ. Health Perspect.* **124**, 281–289 (2016).
36. S. S. Lim *et al.*, A comparative risk assessment of burden of disease and injury attributable to 67 risk factors and risk factor clusters in 21 regions, 1990–2010: A systematic analysis for the global burden of disease study 2010. *Lancet* **380**, 2224–2260 (2012). Corrected in: *Lancet* **381**, 1276 (2013).
37. E. A. Marais, C. Wiedinmyer, Air quality impact of diffuse and inefficient combustion emissions in Africa (DICE-Africa). *Environ. Sci. Technol.* **50**, 10739–10745 (2016).
38. G. R. van der Werf *et al.*, Global fire emissions estimates during 1997–2016. *Earth Syst. Sci. Data* **9**, 697–720 (2017).
39. N. A. Krotkov *et al.*, The version 3 OMI NO₂ standard product. *Atmos. Meas. Tech.* **10**, 3133–3149 (2017).
40. L. Giglio, L. Boschetti, D. P. Roy, M. L. Humber, C. O. Justice, The collection 6 MODIS burned area mapping algorithm and product. *Remote Sens. Environ.* **217**, 72–85 (2018).
41. E. Roteta, A. Bastarrika, M. Padilla, T. Storm, E. Chuvieco, Development of a Sentinel-2 burned area algorithm: Generation of a small fire database for sub-Saharan Africa. *Remote Sens. Environ.* **222**, 1–17 (2019).
42. J. A. Adeniran, R. O. Yusuf, B. S. Fakinle, J. A. Sonibare, Air quality assessment and modelling of pollutants emission from a major cement plant complex in Nigeria. *Atmos. Pollut. Res.* **10**, 257–266 (2019).
43. F. I. Abam, G. O. Unachukwu, Vehicular emissions and air quality standards in Nigeria. *Eur. J. Sci. Res.* **34**, 550–560 (2009).
44. O. N. Maitera, H. Louis, Y. Y. Emmanuel, O. U. Akakuru, E. I. Nosike, Air quality index of CO and NO₂ in ambient air of Jemita/Yola metropolis, Adamawa State, Nigeria. *Adv. Anal. Chem.* **8**, 1–5 (2018).
45. I. F. Chizoruo, O. A. Iheanyichukwu, N. P. Chukwuemeka, A. J. Ikechukwu, Ambient air quality assessment of Orlu, southeastern, Nigeria. *J. Appl. Sci.* **17**, 441–457 (2017).
46. K. L. Njoku, T. J. Rumide, M. O. Akinola, A. A. Adesuyi, A. O. Jolaoso, Ambient air quality monitoring in metropolitan city of Lagos, Nigeria. *J. Appl. Sci. Environ. Manag.* **20**, 178 (2016).
47. J. Bahino *et al.*, A pilot study of gaseous pollutants' measurement (NO₂, SO₂, NH₃, HNO₃ and O₃) in Abidjan, Côte d'Ivoire: Contribution to an overview of gaseous pollution in African cities. *Atmos. Chem. Phys.* **18**, 5173–5198 (2018).
48. FAO, FAO statistics database. <http://www.fao.org/faostat/en/>. Accessed 1 January 2019.
49. A. Gbadegesin, B. B. Olusesi, Effects of land clearing methods on soil physical and hydrological properties in south-western Nigeria. *Environmentalist* **14**, 297–303 (1994).
50. R. N. Yegbeme, H. Kabir, O. H. R. Awoye, J. A. Yabi, A. A. Paraiso, Managing the agricultural calendar as coping mechanism to climate variability: A case study of maize farming in northern Benin, West Africa. *Clim. Risk Manage.* **3**, 13–23 (2014).
51. T. Lavigne, C. Liu, N. Liu, How does the trend in thunder days relate to the variation of lightning flash density? *J. Geophys. Res. Atmos.* **124**, 4955–4974 (2019).
52. C. M. Taylor *et al.*, Frequency of extreme Sahelian storms tripled since 1982 in satellite observations. *Nature* **544**, 475–478 (2017).
53. M. Harel, C. Price, Thunderstorm trends over Africa. *J. Clim.* **33**, 2741–2755 (2020).
54. N. C. G. Hart, R. Washington, R. I. Maidment, Deep convection over Africa: Annual cycle, ENSO, and trends in the hotspots. *J. Clim.* **32**, 8791–8811 (2019).
55. J. P. Messina, B. G. Peter, S. S. Snapp, Re-evaluating the Malawian farm input subsidy programme. *Nat. Plants* **3**, 17013 (2017). Correction in: *Nat. Plants* **3**, 17044 (2017).
56. R. C. Hudman *et al.*, Steps towards a mechanistic model of global soil nitric oxide emissions: Implementation and space based-constraints. *Atmos. Chem. Phys.* **12**, 7779–7795 (2012).
57. J. E. Hickman, E. Dammers, C. Galy-Lacaux, G. R. van der Werf, Satellite evidence of substantial rain-induced soil emissions of ammonia across the Sahel. *Atmos. Chem. Phys.* **18**, 16713–16727 (2018).
58. Y. Chen *et al.*, A pan-tropical cascade of fire driven by El Niño/Southern oscillation. *Nat. Clim. Chang.* **7**, 906–911 (2017).
59. US Energy Information Agency, International energy statistics database. <http://www.eia.gov/international/overview/world>. Accessed 1 March 2019.
60. R. C. R. Abreu *et al.*, The biodiversity cost of carbon sequestration in tropical savanna. *Sci. Adv.* **3**, e1701284 (2017).
61. N. A. Krotkov, OMI/Aura NO₂ cloud-screened total and tropospheric column L3 global gridded 0.25 degree x 0.25 degree V3. https://disc.gsfc.nasa.gov/datacollection/OMINO2d_003.html. Accessed 1 May 2018.
62. C. A. McLinden *et al.*, Improved satellite retrievals of NO₂ and SO₂ over the Canadian oil sands and comparisons with surface measurements. *Atmos. Chem. Phys.* **14**, 3637–3656 (2014).
63. L. N. Lamsal *et al.*, Evaluation of OMI operational standard NO₂ column retrievals using in situ and surface-based NO₂ observations. *Atmos. Chem. Phys.* **14**, 11587–11609 (2014).
64. M. Ossouhou *et al.*, Trends and seasonal variability of atmospheric NO₂ and HNO₃ concentrations across three major African biomes inferred from long-term series of ground-based and satellite measurements. *Atmos. Environ.* **207**, 148–166 (2019).
65. J. Herman *et al.*, A net decrease in the Earth's cloud, aerosol, and surface 340 nm reflectivity during the past 33 yr (1979–2011). *Atmos. Chem. Phys.* **13**, 8505–8524 (2013).
66. P. Castellanos, K. F. Boersma, O. Torres, J. F. de Haan, OMI tropospheric NO₂ air mass factors over South America: Effects of biomass burning aerosols. *Atmos. Meas. Tech.* **8**, 3831–3849 (2015).
67. J. Chimot, T. Vlemmix, J. P. Veefkind, J. F. de Haan, P. F. Levelt, Impact of aerosols on the OMI tropospheric NO₂ retrievals over industrialized regions: How accurate is the aerosol correction of cloud-free scenes via a simple cloud model? *Atmos. Meas. Tech.* **9**, 359–382 (2016).
68. L. Clarisse, C. Clerbaux, F. Dentener, D. Hurtmans, P.-F. Coheur, Global ammonia distribution derived from infrared satellite observations. *Nat. Geosci.* **2**, 479–483 (2009).
69. M. Van Damme *et al.*, Global distributions, time series and error characterization of atmospheric ammonia NH₃ from IASI satellite observations. *Atmos. Chem. Phys.* **14**, 2905–2922 (2014).
70. M. Van Damme *et al.*, Version 2 of the IASI NH₃ neural network retrieval algorithm: Near-real-time and reanalysed datasets. *Atmos. Meas. Tech.* **10**, 4905–4914 (2017).
71. D. Hurtmans *et al.*, FORLI radiative transfer and retrieval code for IASI. *J. Quant. Spectrosc. Radiat. Transf.* **113**, 1391–1408 (2012).
72. G. J. Huffman *et al.*, The TRMM multisatellite precipitation Analysis (TMPA): Quasi-global, multiyear, combined-sensor precipitation estimates at fine scales. *J. Hydrometeorol.* **8**, 38–55 (2007).
73. S. Nicholson *et al.*, Validation of TRMM and other rainfall estimates with a high-density gauge dataset for West Africa. Part II: Validation of TRMM rainfall products. *J. Appl. Meteorol.* **42**, 1355–1368 (2003).
74. S. K. Akagi *et al.*, Emission factors for open and domestic biomass burning for use in atmospheric models. *Atmos. Chem. Phys.* **11**, 4039–4072 (2011).
75. R. M. Hoesly *et al.*, Historical (1750–2014) anthropogenic emissions of reactive gases and aerosols from the community emission data system (CEDS). *Geosci. Model Dev.* **11**, 369–408 (2018).
76. J. E. Dobson, E. A. Bright, P. R. Coleman, R. C. Durfee, B. A. Worley, LandScan: A global population database for estimating populations at risk. *Photogramm. Eng. Remote Sensing* **66**, 849–857 (2000).
77. M. Kumm, M. Taka, J. H. A. Guillaume, Gridded global datasets for gross domestic product and human development index over 1990–2015. *Sci. Data* **5**, 180004 (2018).
78. B. de Foy, Z. Lu, D. G. Streets, L. N. Lamsal, B. N. Duncan, Estimates of power plant NO_x emissions and lifetimes from OMI NO₂ satellite retrievals. *Atmos. Environ.* **116**, 1–11 (2015).
79. C. Jena *et al.*, Estimation of the lifetime of nitrogen oxides over India using SCIAMACHY observations. *Int. J. Remote Sens.* **35**, 1244–1252 (2014).
80. S. Beirle, K. F. Boersma, U. Platt, M. G. Lawrence, T. Wagner, Megacity emissions and lifetimes of nitrogen oxides probed from space. *Science* **333**, 1737–1739 (2011).